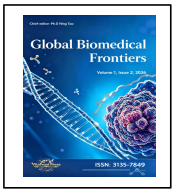
Global Biomedical Frontiers
https://www.vifpress.com/journals/global-biomedical-frontiers



Identification of Novel CAF Target FABP1 and Its Therapeutic Ligand Alitretinoin for Pancreatic Ductal Adenocarcinoma Using Quantitative Proteomics and Molecular Docking

Xiaoyu Bai

Beijing No. 2 High School, Beijing, China

Information

Keywords:
pancreatic ductal adenocarcinoma;
cancer-associated fibroblasts; FABP1;
alitretinoin;
9-cis-retinoic acid;
molecular docking;
drug repurposing

Abstract

Cancer-associated fibroblasts (CAFs) within the tumor microenvironment are major drivers of chemoresistance in pancreatic ductal adenocarcinoma (PDAC). However, specific molecular targets for CAF-directed therapy and clinically available repurposed drugs remain scarce. In the present study, quantitative proteomic data comparing CAFs and normal fibroblasts (NFs) derived from our in-house PDAC dataset were analyzed. Genes significantly upregulated in CAFs and markedly downregulated upon prednisolone exposure were screened. Retinol-metabolizing enzyme ALDH8A1 was identified, whose catalytic product 9-cis-retinoic acid corresponds to the approved drug alitretinoin. Three-dimensional structures of target protein and candidate ligands were retrieved from the RCSB PDB and PubChem databases. SwissDock-based molecular-docking was performed to assess binding affinities between FABP1 and 9-cis-retinoic acid, alongside other retinol-related metabolites and clinically used antitumor agents. Homologous protein FABP5 was included as a control to evaluate subtype-specificity. The MolModa tool was further applied for multidimensional druggability assessment of all FABP1 binding pockets, followed by replicate-docking validation. Our docking results revealed that 9-cis-retinoic acid bound to FABP1 with a binding free energy of −10.542 kcal/mol, representing substantially higher affinity relative to other ligands and FABP5. Pocket3Box was defined as the optimal binding cavity, with the lowest binding free energy of −9.656 kcal/mol in replicate-docking assays, confirming robust and subtype-specific high-affinity interaction. Subsequent cellular transcriptomic experiments demonstrated that 9-cis-retinoic acid potently suppressed activation, pro-tumorigenic secretion and proliferative phenotypes of pancreatic stellate cells, while globally rewiring cellular lipid metabolic homeostasis. These findings provide direct experimental evidence supporting 9-cis-retinoic acid-mediated inhibition of PDAC CAFs. Collectively, FABP1 binds 9-cis-retinoic acid (alitretinoin, an FDA-approved drug with established clinical safety and pharmacokinetic profiles) with high subtype selectivity and ultra-high affinity. This target-drug pairing “FABP1-alitretinoin” establishes a novel drug-repurposing strategy for stroma-targeted intervention in PDAC, which is ready for further in-vitro and in-vivo experimental validation.

Introduction

Pancreatic ductal adenocarcinoma (PDAC), often referred to as the “king of cancers”, is characterized by insidious onset, aggressive metastatic potential and dismal clinical prognosis. The overall 5-year survival rate globally remains below 10 %, and median survival for patients with advanced metastatic disease is merely 6–9 months. Epidemiological projections indicate that PDAC will become the second leading cause of cancer-related mortality worldwide, only exceeded by lung cancer by 2030, highlighting an urgent unmet clinical need. Due to the deep anatomical location of the pancreas and the absence of early-specific symptoms, only approximately 20 % of patients are eligible for curative surgical resection at initial diagnosis. The majority of patients present with locally advanced or metastatic disease at diagnosis and are not candidates for radical surgery. For unresectable PDAC, first-line chemotherapy regimens such as FOLFIRINOX and gemcitabine plus nab-paclitaxel only yield modest survival

Email: Xiaoyu Bai, 28394222@qq.com.

benefits, accompanied by frequent primary or acquired chemoresistance as well as severe systemic adverse events including myelosuppression and gastrointestinal toxicity. Furthermore, PDAC is a typical immune-cold tumor; monotherapy with immune checkpoint inhibitors confers minimal clinical benefit. Therefore, substantial bottlenecks persist within current therapeutic frameworks for PDAC.

Exuberant fibrotic stroma is a hallmark pathological feature distinguishing PDAC from most other solid malignancies. Dense collagen fibers form a physical barrier that impedes infiltration of chemotherapeutic agents and antitumor immune effector cells into tumor parenchyma, serving as a fundamental microenvironmental basis for therapeutic resistance. Cancer-associated fibroblasts (CAFs) constitute the most abundant stromal cell population within the PDAC tumor microenvironment (TME) and exhibit prominent cellular heterogeneity, differentiating into functional subsets including inflammatory CAFs, myofibroblastic CAFs (myCAFs) and antigen-presenting CAFs. Among these, myCAFs represent the core pro-tumorigenic subpopulation. Activated pro-tumorigenic CAFs facilitate PDAC malignant progression through three primary mechanisms: first, massive secretion of type I/IV collagen remodels the extracellular matrix and exacerbates fibrotic barriers; second, release of chemokines and growth factors establishes an immunosuppressive microenvironment and drives effector T-cell exhaustion; third, metabolic symbiosis with tumor cells via the reverse Warburg effect provides nutritional support for cancer cell proliferation and DNA-damage repair. Collectively, these processes amplify tumor aggressiveness and sustain chemotherapeutic resistance.

Current CAF-targeting therapeutic strategies have achieved limited clinical translational success. Most existing studies focus on CAF-secretory signaling or collagen biosynthesis pathways, whereas CAF-intrinsic metabolic programs sustaining persistent activation and survival remain insufficiently explored. The lack of precise screening and validation of CAF-specific metabolic nodes constitutes a major obstacle for developing stroma-directed therapeutics. Compared with de-novo small-molecule drug discovery, repurposing already-approved agents against CAF-specific metabolic targets offers unique advantages including shortened research-and-development cycles, well-characterized safety profiles and lower clinical-translation barriers. Given the above-mentioned clinical demands and existing research gaps, the present study aimed to identify specific metabolic targets maintaining CAF activation and pro-tumorigenic functions, and to match these targets with clinically approved drugs. We sought to establish a low-toxicity, rapidly translatable novel intervention strategy targeting tumor stroma, providing new insights to overcome PDAC chemoresistance and improve patient outcomes.

1 Materials and Methods

1.1 Screening criteria for differential proteomic candidates

An in-house quantitative proteomic dataset comparing CAFs and normal fibroblasts (NFs) was utilized. Two-fold filtering thresholds were applied: (1) significantly increased expression in CAFs relative to NFs ($log_2FC>0$, statistically significant); (2) significantly decreased expression in prednisolone-treated CAFs (CAF_P) relative to untreated CAFs ($log_2FC<0$, statistically significant). Genes satisfying both criteria were included for subsequent pathway functional annotation.

1.2 Preprocessing of target-protein and ligand structures

Three-dimensional crystal structures of target proteins were retrieved from the RCSB PDB database. Standardized SMILES structures of all tested ligands were obtained from the PubChem database. Energy minimization was performed for all ligands prior to molecular-docking simulations.

1.3 Molecular-docking parameter settings and affinity grading criteria

Molecular simulations of ligand-protein interactions were implemented on the SwissDock web server. Binding free energy ΔG (unit: kcal/mol) was adopted as the readout for ligand-protein binding affinity. Grading criteria for binding affinity are summarized in **Table 1**.

Table 1. Grading criteria for ligand-protein binding affinity based on binding free energy

Binding free energy ΔG (kcal/mol)	Affinity grade
≤ −10.0	Ultra-high affinity
−10.0 ~ −7.0	High affinity
−7.0 ~ −5.0	Moderate affinity
> −5.0	Low affinity

Footnote: ΔG, binding free energy.

Unified docking simulation parameters: only chain A of the target protein was retained; all heteroatoms were removed from protein structures. The search box for binding sites was centered at coordinates 30, −2, 4 Å with spatial dimensions of 20 Å × 20 Å × 20 Å; exhaustiveness = 20.

1.4 Multiparameter druggability evaluation of binding pockets and replicate-docking validation

To further verify the reliability of FABP1-9-cis-retinoic acid binding affinity and pinpoint the optimal ligand-binding cavity, the MolModa tool was employed for multidimensional druggability assessment of all predicted FABP1 pockets. Evaluated parameters included Alphasphere druggability score, total solvent-accessible surface area (Total SASA), polar/nonpolar solvent-accessible surface area, cavity volume, mean local hydrophobic density, mean Alphasphere radius, hydrophobicity score, polarity score, charge score and Alphasphere density. The top-four ranked pockets (Pocket1Box, Pocket2Box, Pocket3Box, Pocket8Box) according to comprehensive druggability scores were subjected to multiple rounds of replicate docking. Mean binding free energy, optimal-pose binding free energy and data dispersion for each pocket were calculated to comprehensively evaluate binding stability and pocket-specific ligand-binding preference.

Unified docking simulation parameters: consider visible molecules; consider selected molecules; spatial dimension 20 Å × 20 Å × 20 Å; number of processors = 21; exhaustiveness = 32; maximum rotatable bonds = 15; only the highest-score pose was retained for each complex.

1.5 Phenotypic observation under in-vitro pharmacological intervention

Immortalized human pancreatic stellate cells (ihPSCs) with comparable confluency and cell density were seeded in 100 mm cell-culture dishes. Cells were divided into two groups: solvent-control group treated with 0.1 % (v/v) dimethyl sulfoxide (DMSO), and treatment group exposed to 0.05 μM 9-cis-retinoic acid. The final DMSO concentration was kept identical across groups to eliminate solvent interference. Cells were incubated at 37 °C with 5 % CO_2 for 24 h. Overall cellular growth status and density were visually inspected under an inverted microscope, and bright-field micrographs were acquired.

1.6 Bioinformatic analysis of transcriptome sequencing

Cells from the 0.1 % (v/v) DMSO solvent-control group and the 0.05 μM 9-cis-retinoic-acid-treated group were harvested. Final DMSO concentrations were matched between groups. After 72 h incubation at 37 °C, 5 % CO_2, samples were submitted for standard transcriptome sequencing and bioinformatic analysis.

2 Results

2.1 Identification of candidate target protein FABP1

Fatty-acid-binding proteins (FABPs) constitute a family of ~15 kDa intracellular lipid-transport proteins participating in cytosolic fatty-acid trafficking and lipid-signaling regulation, comprising 12 distinct isoforms. Our proteomic data demonstrated that only three FABP isoforms, namely FABP1, FABP3 and FABP5, were significantly upregulated in CAFs. Their fold-change values are listed in **Table 2**.

Table 2. log_2 fold-change values of FABP family proteins in CAFs compared with NFs

Gene symbol	CAF vs NF log_2FC
FABP1	0.994648833
FABP3	0.65119356
FABP5	0.270932505

Footnote: FC, fold-change. Gene symbols represent mRNA transcripts and are italicized.

As shown in Table 2, FABP1 exhibited the highest upregulation magnitude among the three isoforms. FABP5 has been well-documented to exert pro-oncogenic roles in multiple solid tumors yet faces substantial limitations in clinical translation. Previous studies on FABP1 mainly focused on hepatic lipid metabolism, non-alcoholic fatty-liver disease and liver-injury biomarkers; its biological function in PDAC-associated CAFs has not been reported to date. Structurally, FABP1 harbors a large ligand-binding cavity with a volume of 600–800 $Å^3$, conferring favorable accommodation capacity for hydrophobic small molecules. Integrating expression magnitude, research gaps and structural suitability, FABP1 was selected as the core target protein for subsequent investigation.

2.2 Identification of retinol-metabolism-related candidate ALDH8A1

In total, eight genes satisfied our dual filtering criteria. These candidates were functionally categorized into extracellular-matrix components, vesicular-trafficking regulators, metalloproteinases and oxidoreductases (**Table 3**). Among them, ALDH8A1, an oxidoreductase in retinol-metabolism pathways, displayed the largest downregulation magnitude ($log_2FC = -1.78734$) upon prednisolone treatment, indicating high sensitivity of ALDH8A1 expression to prednisolone and its key regulatory role in CAF metabolic reprogramming.

Table 3. Differential genes satisfying dual screening criteria: expression changes and functional annotations

Gene symbol	Full gene name	CAF_P vs CAF log_2FC	Functional category
ALDH8A1	Aldehyde dehydrogenase 8 family member A1	−1.78734	Retinol metabolism / oxidoreductase
NID1	Nidogen-1	−0.28618	Extracellular-matrix component
MFAP2	Microfibril-associated protein 2	−1.47637	Extracellular-matrix synthesis / elastic-fibre assembly
ECM1	Extracellular-matrix protein 1	−0.53335	Extracellular-matrix homeostasis regulation
SCRN3	Secernin-3	−0.51616	Cytoskeleton regulation / vesicular trafficking
MEP1A	Meprin A subunit α	−0.46145	Metalloproteinase
PLXDC1	Plexin domain-containing protein 1	−0.82957	Cytoskeleton / angiogenesis regulation
LRRC17	Leucine-rich repeat-containing 17	−1.3448	Extracellular matrix / signal transduction

Footnote: FC, fold-change. Gene symbols are italicized.

2.3 ALDH8A1 specifically mediates biosynthesis of 9-cis-retinoic acid

According to annotations from the KEGG and Reactome pathway databases, ALDH8A1 acts as a terminal oxidase downstream within retinol-metabolism cascades, specifically catalyzing oxidation of 9-cis-retinal to 9-cis-retinoic acid, representing the final catalytic step in vitamin A activation. 9-cis-retinoic acid serves as an endogenous natural ligand for nuclear receptor RXR and constitutes the pharmacologically active moiety of FDA-approved drug alitretinoin. Prednisolone-induced downregulation of ALDH8A1 indicates aberrant retinol-metabolic reprogramming in CAFs. Given that the terminal metabolite corresponds to a marketed pharmaceutical agent, this pathway possesses high potential for drug-repurposing research.

2.4 Core molecular transformation within retinol-metabolism pathways

Table 4. Transformation relationships of key molecules in retinol-metabolism pathways

Parent molecule	Catalytic product	Upstream precursor	Core catalytic enzyme
Vitamin A (all-trans-retinol)	9-cis-retinal	β-carotene / retinyl ester	RDH/ADH dehydrogenases (with isomerization and oxidation activities)
9-cis-retinal	9-cis-retinoic acid	9-cis-retinol derived from vitamin A	ALDH8A1
9-cis-retinoic acid	No further oxidative metabolites	9-cis-retinal	ALDH8A1
ATRA (all-trans-retinoic acid)	No further oxidative metabolites	all-trans-retinal	ALDH1A1/1A2/1A3

2.5 Multidimensional molecular docking verifies high-affinity binding between FABP1 and 9-cis-retinoic acid

Three control sets were established: retinol-pathway metabolite controls, clinical antitumor-drug controls and homologous-protein (FABP5) isoform controls. Binding-free-energy results for all ligand-protein pairs are summarized in **Table 5**.

Table 5. Summary of binding free energies for tested ligand-target-protein pairs

Ligand name	Target protein	ΔG (kcal/mol)	Affinity grade
9-cis-retinoic acid	FABP1	−10.345	Ultra-high affinity
Vitamin A	FABP1	−7.737	High affinity
9-cis-retinal	FABP1	−9.826	High affinity
ATRA	FABP1	−7.460	High affinity
Curcumin	FABP1	−8.875	High affinity
Aspirin	FABP1	−6.498	Moderate affinity
Vitamin C	FABP1	−4.986	Low affinity
9-cis-retinoic acid	FABP5	−5.391	Moderate affinity

Footnote: ΔG, binding free energy.

2.6 Multiparameter druggability evaluation of FABP1 binding pockets and identification of optimal binding regions

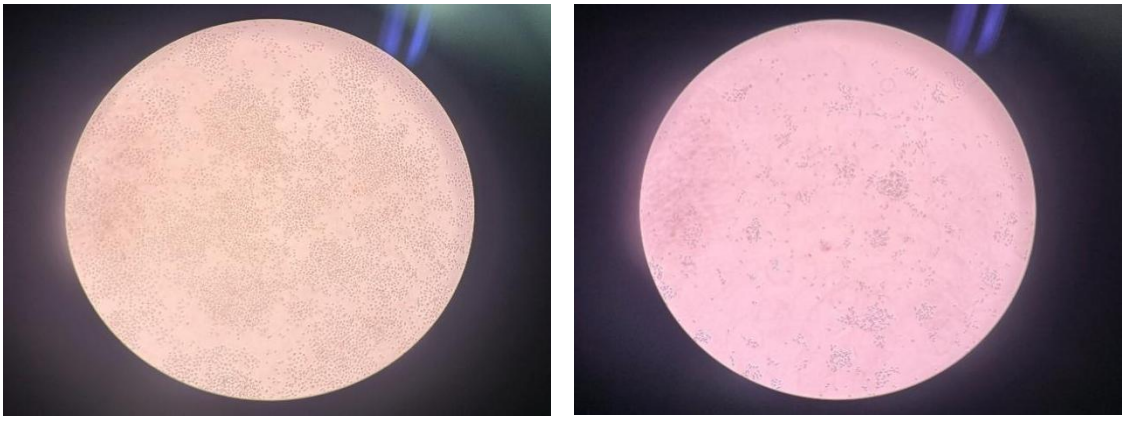
To exclude systematic bias introduced by single-software docking and clarify pocket-dependent affinity and druggability for 9-cis-retinoic acid-FABP1 interaction, the MolModa tool predicted all putative FABP1 binding cavities. The top-four druggability-ranked pockets (Pocket1, Pocket2, Pocket3, Pocket8) were selected for multiple replicate-docking assays. Key druggability metrics and docking outputs are presented in **Table 6**.

Table 6. Druggability parameters and replicate-docking outcomes for top-four predicted pockets

Parameter / Pocket ID	P1	P2	P3	P8
Mean binding free energy (kcal/mol)	−9.77	−10.20	−9.21	−9.09
Optimal-pose binding free energy (kcal/mol)	−9.829	−10.542	−9.656	−9.188
Druggability score	0.843	0.734	0.953	0.867
Cavity volume (Å³)	888.5	750.3	787.3	1084.5
Nonpolar SASA	173.0	165.4	185.9	246.4
Hydrophobicity score	51.47	51.04	50.65	49.91
Polarity score	13.0	11.0	11.0	14.0
Alphasphere density	6.62	6.09	6.08	8.32

Footnote: Center coordinates for binding-site search boxes: P1: 53, −2, −45 Å; P2: 20, −4, 5 Å; P3: 16, −3, −82 Å; P5: 15, −7, −23 Å. SASA, solvent-accessible surface area.

2.7 Cellular phenotypic outcomes under in-vitro pharmacological intervention



(A) **(B)**

Fig. 1 Bright-field micrographs of immortalized human pancreatic stellate cells (ihPSCs). (A) Solvent-control group treated with 0.1 % (v/v) DMSO. (B) 0.05 μM 9-cis-retinoic acid-treated group.

The solvent-control group (0.1 % v/v DMSO) exhibited robust cell growth and high confluency; cells displayed typical elongated spindle-shaped morphology with full cell bodies and dense uniform monolayers. In contrast, the 0.05 μM 9-cis-retinoic-acid-treated group exhibited markedly suppressed proliferation and substantially reduced confluency. Treated cells became sparsely distributed, partially transformed from spindle-shaped into polygonal or rounded morphology and failed to form compact monolayers, suggesting proliferation arrest or early cellular damage induced by 9-cis-retinoic acid.

2.8 Transcriptomic validation of 9-cis-retinoic-acid-mediated suppression of pancreatic stellate-cell pro-tumorigenic phenotypes

After 72 h treatment with 0.05 μM 9-cis-retinoic acid, transcriptome sequencing was performed on ihPSC cells. Key differentially expressed genes associated with phenotypic alterations are summarized in **Table 7**.

Table 7. Differentially expressed genes linked to 9-cis-retinoic-acid-driven phenotypic suppression in pancreatic stellate cells

Gene symbol	log_2FC	Adjusted P-value	Functional role / marker property	Validation dimension
TAGLN	−2.27	7.38×10^{-25}	Myofibroblast-activation marker; cytoskeleton-associated protein upregulated upon CAF activation, core marker for CAF transition toward pro-tumorigenic phenotypes	Suppression of CAF-activation phenotype
TPM1	−1.49	6.72×10^{-33}	Cytoskeleton-remodeling marker; tropomyosin stabilises cytoskeleton and contractility; its downregulation reflects blockade of CAF morphological and functional reprogramming	Suppression of CAF-activation phenotype
FGF1	−2.32	5.68×10^{-23}	Pro-tumorigenic growth factor; fibroblast growth factor 1, a major CAF-secreted pro-mitogen	Suppression of pro-tumorigenic secretory phenotype
CTGF	−1.01	1.64×10^{-8}	Core profibrotic mediator; connective-tissue growth factor driving fibrosis and extracellular-matrix deposition	Suppression of pro-tumorigenic secretory phenotype
CYR61	−1.16	3.35×10^{-22}	Profibrotic factor; cysteine-rich angiogenic inducer 61, participating in ECM remodelling and pro-angiogenic effects	Suppression of pro-tumorigenic secretory phenotype
DLL4	−3.53	5.27×10^{-11}	Notch-pathway ligand; mediates Notch signaling to promote tumor angiogenesis and cancer-cell stemness	Suppression of pro-tumorigenic secretory phenotype
WNT7A	−1.35	9.52×10^{-13}	Wnt-pathway ligand; activates canonical Wnt/β-catenin signaling to boost tumor proliferation and invasion	Suppression of pro-tumorigenic secretory phenotype

Gene symbol	log_2FC	Adjusted P-value	Functional role / marker property	Validation dimension
WNT7B	−1.27	4.42×10^{-12}	Wnt-pathway ligand; functionally analogous to WNT7A, synergistically facilitating tumor progression	Suppression of pro-tumorigenic secretory phenotype
WNT5B	−1.05	1.39×10^{-11}	Wnt-pathway ligand; mediates noncanonical Wnt signaling to promote tumor-cell migration and invasion	Suppression of pro-tumorigenic secretory phenotype
CDK5R1	−1.10	1.98×10^{-3}	Cell-cycle activator; regulatory subunit of CDK5 promoting cell-cycle progression	Proliferation inhibition and cell-cycle arrest
CDKN2B	+1.20	3.25×10^{-4}	Cell-cycle-inhibitory factor (G1-phase arrest); p15INK4b, canonical negative CDK4/6 regulator	Proliferation inhibition and cell-cycle arrest
RB1CC1	+1.02	5.77×10^{-3}	Cell-cycle-inhibition-related factor; RB1-inducible coiled-coil 1, involved in RB1/p53-driven cell-cycle arrest	Proliferation inhibition and cell-cycle arrest
ADAMTS1	−1.57	2.28×10^{-15}	Matrix-remodeling protease; ADAM metallopeptidase with thrombospondin type 1 motif 1, mediates ECM degradation and remodelling	Matrix remodelling and angiogenesis regulation
APLN	−2.80	9.11×10^{-25}	Pro-angiogenic factor; apelin, a key CAF-secreted angiogenic mediator	Matrix remodelling and angiogenesis regulation
DHRS3	+2.18	4.55×10^{-34}	Retinoic-acid-signaling activation readout; dehydrogenase/reductase SDR family member 3, negative-feedback regulator of retinoic-acid signaling; its upregulation serves as a classic marker for intracellular retinoid-drug bioactivity	Pharmacological-effect validation
DHCR24	−1.76	1.45×10^{-40}	Key cholesterol-biosynthetic enzyme; 24-dehydrocholesterol reductase catalyses the final step of cholesterol synthesis	Global lipid-metabolism reprogramming
DHCR7	−1.44	1.26×10^{-19}	Key cholesterol-biosynthetic enzyme; 7-dehydrocholesterol reductase, rate-limiting cholesterol-synthesis component	Global lipid-metabolism reprogramming
LSS	−1.31	3.12×10^{-13}	Key cholesterol-biosynthetic enzyme; lanosterol synthase, essential node in cholesterol biogenesis	Global lipid-metabolism reprogramming
MVK	−1.29	2.22×10^{-9}	Key enzyme for cholesterol/isoprenoid biosynthesis; mevalonate kinase in the mevalonate pathway	Global lipid-metabolism reprogramming
SQLE	−1.17	8.74×10^{-18}	Rate-limiting cholesterol-biosynthetic enzyme; squalene epoxidase	Global lipid-metabolism reprogramming
HMGCS1	−1.09	2.50×10^{-9}	Key cholesterol-biosynthetic enzyme; HMG-CoA synthase 1 initiating the mevalonate pathway	Global lipid-metabolism reprogramming
FDPS	−1.05	1.06×10^{-12}	Downstream mevalonate-pathway enzyme for cholesterol/isoprenoid synthesis; farnesyl diphosphate synthase	Global lipid-metabolism reprogramming
ABCA1	+5.34	2.93×10^{-10}	Lipid-efflux transporter; ATP-binding-cassette transporter A1 mediates cellular cholesterol/phospholipid efflux to apolipoprotein AI, core mediator of lipid clearance	Global lipid-metabolism reprogramming
ANGPTL4	+2.24	1.61×10^{-44}	Lipid-metabolism regulator; angiopoietin-like 4 modulates lipoprotein lipase activity and promotes lipolysis	Global lipid-metabolism reprogramming

Footnote: FC, fold-change. Gene symbols are italicized. Adjusted P-value, padj.

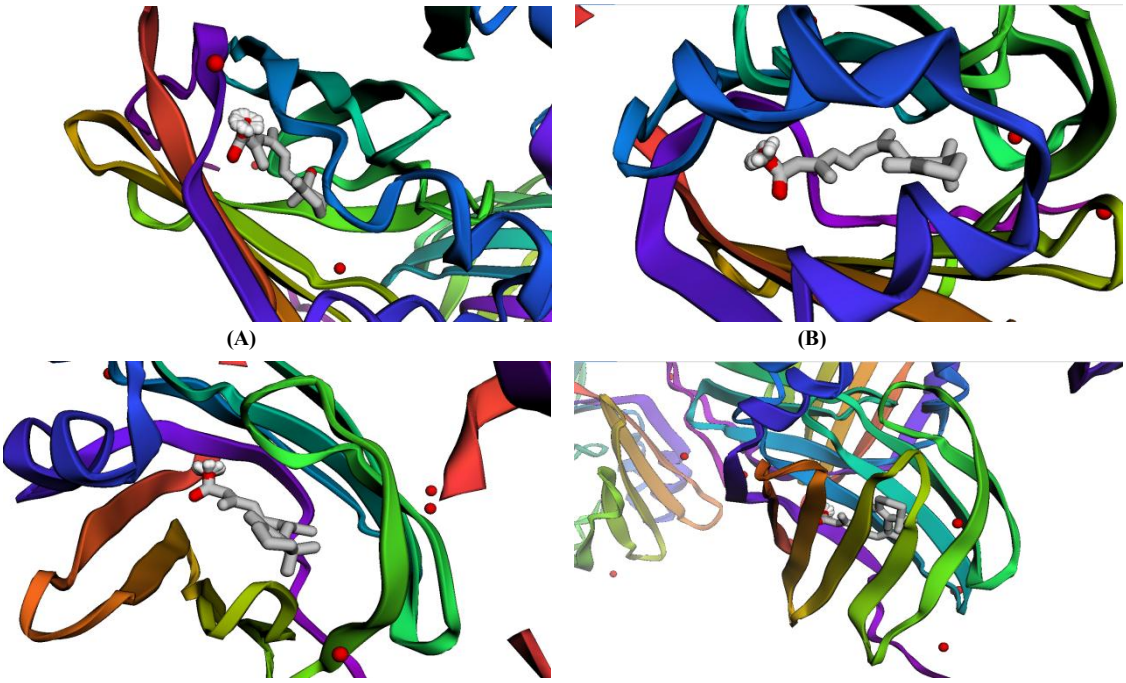


Fig. 2 Representative binding poses of 9-cis-retinoic acid within the Pocket3 cavity of FABP1. (A-D) Different visual perspectives of ligand-protein complex structure.

3 Discussion

3.1 Broad capacity of FABP1 for binding diverse hydrophobic small-molecule ligands

Among seven tested ligands, only vitamin C exhibited low-affinity binding toward FABP1. The remaining six ligands achieved high-affinity binding status, five of which displayed binding free energies below −8.0 kcal/mol. This observation aligns with the structural feature of the large hydrophobic cavity within FABP1. Computational docking collectively supports that FABP1 can broadly accommodate hydrophobic lipid-like small molecules, rendering it a promising scaffold protein for small-molecule therapeutic development.

3.2 Isoform-specific binding preference of FABP1 toward 9-cis-retinoic acid

Three control dimensions (metabolic-pathway substrates, clinical drugs and homologous isoform) collectively validated binding specificity.

3.2.1 Gradient control of pathway substrates

Comparison across retinol-metabolism intermediates demonstrated that the terminal product 9-cis-retinoic acid achieved the lowest binding free energy toward FABP1; binding affinity increased progressively along the ALDH8A1-driven oxidative cascade. This pattern indicates that FABP1 does not indiscriminately sequester pathway intermediates but selectively enriches the ALDH8A1-catalysed terminal bioactive product 9-cis-retinoic acid.

3.2.2 Parallel control of clinical agents

Compared with ATRA, curcumin, aspirin and vitamin C, 9-cis-retinoic acid exhibited superior binding strength against FABP1. Thermodynamically, these results highlight the pharmacological potential of alitretinoin as a FABP1-targeting agent relative to multiple existing antitumor adjuvant drugs.

3.2.3 Homologous-isoform specificity validation

Homologous isoform FABP5 only exhibited moderate-affinity interaction with 9-cis-retinoic acid. The binding-free-energy difference reached 4.95 kcal/mol, corresponding to an approximately 4 000-fold difference in binding affinity. This finding indicates that FABP5 cannot functionally compensate for 9-cis-retinoic-acid capture by FABP1. Therefore, FABP1-targeting strategies possess favorable isoform selectivity and reduced off-target risks.

3.3 Comprehensive analysis of binding pockets and identification of optimal cavities

All four high-potential pockets (Pocket1, Pocket2, Pocket3, Pocket8) supported stable binding of 9-cis-retinoic acid, with mean binding free energies ranging from −10.20 kcal/mol to −9.09 kcal/mol, substantially exceeding nonspecific superficial surface depressions. The rank order of ligand-binding strength was: Pocket2 > Pocket1 > Pocket3 > Pocket8. Pocket2 yielded the optimal-pose binding free energy as low as −10.542 kcal/mol, representing the strongest ligand-protein interaction.

Pocket2 and Pocket3 presented the lowest Alphasphere density with compact deep cavities, which facilitate ligand-protein induced-fit effects. Pocket8 possessed the largest cavity volume and elevated Alphasphere density; its open inner space conferred weak ligand enclosure, hence relatively inferior affinity. All four pockets maintained comparable hydrophobic scores (~50), supplying sufficient hydrophobic interactions. Pocket1 contained the most polar residues; Pocket3 displayed well-balanced hydrophobic-to-polar residue ratios; Pocket2 generated strong hydrophobic interactions relying on its compact cavity architecture.

From a druggability perspective, Pocket3 achieved the highest druggability score (0.953), followed by Pocket8 (0.867), Pocket1 (0.843), whereas Pocket2 obtained a moderate-to-good druggability score of 0.734.

Collectively, ligand-binding strength is not dictated solely by cavity volume or total hydrophobic surface area but is synergistically governed by cavity compactness, local physicochemical microenvironment and complementarity with ligand molecular geometry. When prioritising raw binding affinity, Pocket2 represents the optimal binding site for 9-cis-retinoic acid. Oriented toward downstream small-molecule drug development and balancing druggability and physicochemical balance, Pocket3 was identified as the overall optimal cavity. Accordingly, the optimal Pocket3 pose (binding free energy −9.656 kcal/mol) was selected as the primary starting conformation for subsequent molecular-dynamics simulations and pharmacophore modelling. The high-affinity Pocket2 pose was retained as a control for comparative analyses of binding modes between high-affinity and moderately druggable cavities.

3.4 9-cis-retinoic acid exerts suppressive effects on pancreatic stellate cells

Bright-field microscopy showed vigorous proliferation and dense monolayers in solvent-control ihPSCs with typical elongated spindle morphology. By contrast, 9-cis-retinoic-acid-treated cells displayed markedly reduced confluency, altered cell shape, sparse distribution and failure to form compact monolayers, pointing to proliferation arrest or early cellular damage. These morphological observations demonstrate potent inhibitory activity of 9-cis-retinoic acid against pancreatic stellate-cell growth.

3.5 9-cis-retinoic acid suppresses pro-tumorigenic phenotypes and rewires lipid-metabolism homeostasis in pancreatic stellate cells

Transcriptome sequencing identified 554 significantly differentially expressed genes ($|\log_2 FC|>1$, adjusted P-value < 0.05) after 72 h 0.05 μM 9-cis-retinoic-acid exposure in ihPSCs. Multiple dimensions including CAF-activation repression, attenuation of pro-tumorigenic secretion, proliferation suppression, cell-cycle arrest, retinoic-acid-signaling activation and global lipid-metabolic reprogramming jointly confirmed inhibitory bioactivity of 9-cis-retinoic acid toward pancreatic stellate cells.

3.5.1 Suppression of CAF-activation phenotypes

Markers of myofibroblastic activation TAGLN and cytoskeleton-remodelling gene TPM1 were significantly downregulated upon treatment. TAGLN constitutes a core marker for CAF transition toward pro-tumorigenic myofibroblastic status; its pronounced downregulation indicates that 9-cis-retinoic acid effectively reverses CAF activation. Repressed TPM1 expression further corroborates blockade of CAF morphological and functional reprogramming.

3.5.2 Suppression of pro-tumorigenic secretory phenotypes

CAF-derived pro-tumorigenic growth factor FGF1, core profibrotic mediator CTGF and profibrotic cytokine CYR61 were drastically downregulated. Moreover, Notch-pathway ligand DLL4 and Wnt-pathway ligands WNT7A, WNT7B and WNT5B all exhibited significant repression. These secreted effectors compose the central signaling network mediating CAF-driven tumor proliferation, invasion and fibrotic-barrier construction. Their coordinated downregulation demonstrates that 9-cis-retinoic acid disrupts the pro-tumorigenic secretory niche established by CAFs.

3.5.3 Proliferation suppression and cell-cycle arrest

Cell-cycle-activator gene CDK5R1 was significantly downregulated, whereas cell-cycle-inhibitory genes CDKN2B and RB1CC1 were significantly upregulated. CDKN2B is a well-established negative regulator enforcing G1-phase cell-cycle arrest. Combined repression of CDK5R1 and induction of CDKN2B/RB1CC1 suggest that 9-cis-retinoic acid arrests cell-cycle progression at the G1/S checkpoint and impedes stellate-cell proliferation.

3.5.4 Matrix remodelling and angiogenesis modulation

Matrix-remodeling protease ADAMTS1 and pro-angiogenic factor APLN were markedly downregulated. ADAMTS1 participates in extracellular-matrix degradation and reconstruction, and APLN is a critical CAF-secreted pro-angiogenic mediator. Their repression implies diminished CAF capacity to support matrix remodelling and tumor angiogenesis.

3.5.5 Validation of intracellular pharmacological activation

Strong upregulation of retinol-metabolic enzyme DHRS3 served as a molecular readout for activated retinoic-acid signaling. DHRS3 encodes a key negative-feedback component downstream of retinoic-acid cascades; its robust induction represents a canonical signature of intracellular retinoid-drug bioavailability, verifying successful cellular uptake and target-pathway activation by 9-cis-retinoic acid.

3.5.6 Global reprogramming of lipid-metabolism homeostasis

9-cis-retinoic acid induced widespread remodelling of lipid homeostasis in stellate cells. Multiple key cholesterol-biosynthetic genes (DHCR24, DHCR7, LSS, MVK, SQLE, HMGCS1, FDPS) were coordinately repressed. By contrast, lipid-efflux transporter ABCA1 and lipolysis-regulatory factor ANGPTL4 were strongly upregulated. This dual regulatory pattern — inhibition of cholesterol biosynthesis concurrent with enhanced lipid efflux — demonstrates global blockade of lipogenic programs and promotion of lipid clearance in CAFs. Given the canonical function of FABP1 as an intracellular fatty-acid/lipid chaperone, this lipid-metabolic rewiring forms a functional logical closure with our molecular-docking prediction that 9-cis-retinoic acid acts via FABP1-dependent lipid-metabolism modulation.

3.6 FABP1 represents an original and underexplored stromal target for PDAC-associated CAFs

Previous literature only links FABP1 with hepatic lipid homeostasis and clinical biomarkers for liver injury and fatty-liver disease. To our knowledge, no prior publications have investigated FABP1 within the context of "FABP1 + pancreatic ductal adenocarcinoma + CAF", highlighting its prominent original innovation value. Distinct from FABP5 (extensively studied yet facing translational obstacles), FABP1 possesses a unique spacious cavity capable of accommodating diverse hydrophobic small-molecule compounds and therefore harbours diversified drug-development potential.

3.7 Theoretical basis for ultra-high-affinity interaction between FABP1 and 9-cis-retinoic acid

The observed binding free energy of −10.345 kcal/mol reflects rare ultra-high-affinity natural ligand-protein interaction, a magnitude commonly seen in co-evolved substrate-enzyme or hormone-receptor pairs. This suggests 9-cis-retinoic acid may serve as the physiological optimal endogenous ligand for FABP1. Our three-dimensional control system robustly supports this conclusion:

1. Gradient control along metabolic cascades: binding-affinity shifts align with the ALDH8A1-catalysed oxidative sequence; the binding pocket specifically recognises the molecular geometry conferred by the 9-cis double bond.
2. Parallel clinical-drug control: intermolecular interactions formed by 9-cis-retinoic acid surpass multiple existing antitumor adjuvant agents.
3. Homologous-isoform control: ultra-high-affinity binding is uniquely observed for FABP1, lowering off-target risks for FABP1-directed therapeutics.

Considering the core intracellular lipid-trafficking function of FABP1, we hypothesise that physiological FABP1 function consists of binding and stabilising cytosolic hydrophobic 9-cis-retinoic acid, thereby tuning downstream RXR nuclear-receptor signaling strength.

3.8 Cross-platform validation of high-affinity interaction and pocket-selection rationale

Multipocket replicate docking across independent computational workflows further corroborated our primary findings and mitigated false-positive risks originating from single-search-box parameters or stochastic docking runs. Pocket3 was selected as the primary cavity for molecular-dynamics and pharmacophore modelling owing to its superior druggability and balanced physicochemical properties, adopting its optimal-pose conformation (−9.656 kcal/mol) as a reliable starting structure. Pocket2 with maximum binding affinity (−10.542 kcal/mol) was retained as a comparator for contrasting binding modes and molecular forces between high-affinity and moderately druggable cavities. Our dual-pocket analytical strategy simultaneously maximises binding-strength readout and prioritises small-molecule drug-developability.

3.9 Translational merits of alitretinoin drug-repurposing

A major translational highlight of this work is that 9-cis-retinoic acid corresponds to the marketed agent alitretinoin. It circumvents de-novo drug discovery and preclinical safety assessment and enables immediate advancement to functional in-vitro/in-vivo validation. Four major translational advantages are summarised below:

1. Comprehensive clinical-safety database: Alitretinoin received FDA approval in 1999 for Kaposi's sarcoma and European marketing authorisation in 2008 for chronic eczema. Decades of clinical application have accumulated complete safety records. Therapeutic plasma concentrations ranging 0.1–0.5 μM produce only mild-to-moderate adverse events; routine clinical dosing achieves saturation of FABP1 target (dissociation constant Kd = 10–100 nM).
2. Well-characterised pharmacokinetic profile: Oral bioavailability reaches 60–80 % with in-vivo half-life of 2–10 h. Once-daily dosing facilitates combinatorial regimens alongside chemotherapy, immunotherapy or radiotherapy.
3. Favourable pharmacoeconomic profile: Original patents have expired; generic formulations are widely available at low clinical cost.
4. Pre-existing antitumor-indication basis: Alitretinoin already bears an oncological indication. The present study adds a novel CAF-targeting stromal-modulatory mechanism and expands its therapeutic scope for solid malignancies.

3.10 Rationale for unaltered FABP1 transcript levels and functional-pathway logical linkage

Notably, FABP1 mRNA expression was not significantly altered in transcriptomic datasets. Two plausible explanations are proposed. First, ihPSC immortalised pancreatic stellate cells used herein exhibit low basal FABP1 expression, potentially below RNAseq detection thresholds. Published evidence reports robust FABP1 upregulation in primary activated PDAC CAFs; follow-up experiments in primary CAF isolates are warranted. Second, the principal action of 9-cis-retinoic acid consists of binding and inhibiting lipid-transport function of pre-existing FABP1 protein. Functional protein inhibition does not necessarily drive prominent transcriptional changes of FABP1 mRNA, consistent with our docking-supported direct protein-ligand-binding mode. Despite the absence of FABP1 transcriptional perturbation, 9-cis-retinoic acid profoundly remodels lipid-metabolism pathways that act downstream of FABP1-mediated intracellular lipid trafficking. These downstream transcriptomic alterations indirectly support engagement of the FABP1-centred lipid-regulatory axis by drug treatment.

3.11 Concluding remarks

FABP1 is the most strongly upregulated FABP-family isoform in CAFs, with previously undescribed biological roles within the PDAC tumor microenvironment. Its large hydrophobic internal binding pocket enables efficient engagement with retinoid-like small molecules, qualifying FABP1 as an original stromal-target candidate. Dual-threshold proteomic screening identifies ALDH8A1 as the most substantially downregulated metabolic enzyme upon prednisolone exposure. ALDH8A1 specifically catalyses biosynthesis of 9-cis-retinoic acid, and retinol-metabolism cascades represent a metabolic vulnerability sustaining CAF activation. Multiple sets of molecular-docking simulations confirm ultra-high-affinity binding between FABP1 and 9-cis-retinoic acid with clear isoform-selective target recognition, whereas homologous isoform FABP5 cannot recapitulate this interaction. 9-cis-retinoic acid corresponds to clinically approved alitretinoin with established safety and pharmacokinetic profiles and high clinical accessibility. Multiparameter pocket analysis identifies Pocket3 as the overall optimal cavity with the highest druggability score for follow-up molecular-simulation research. Transcriptomic sequencing demonstrates that 9-cis-retinoic acid exerts multiple inhibitory effects on pancreatic stellate cells in-vitro: suppressing CAF activation, dampening pro-tumorigenic secretory outputs, restraining proliferation, inducing cell-cycle arrest and attenuating CAF-driven matrix remodelling and pro-angiogenic capacity. Significant upregulation of retinoic-acid-signalling marker DHRS3 confirms effective intracellular drug delivery and endogenous retinoid-pathway activation. Global lipid-metabolism rewiring — coordinated repression of cholesterol-biosynthetic programs together with sharp induction of lipid-efflux transporter ABCA1 — forms a functional-pathway closure with FABP1-dependent intracellular lipid trafficking. Collectively, the target-drug pairing "FABP1-alitretinoin" combines novel target discovery, ultra-high-molecular-affinity ligand interaction and high clinical-translation potential. This work establishes a readily testable drug-repurposing framework for stroma-oriented therapeutic intervention against pancreatic ductal adenocarcinoma.

References

[1] Joint Meeting of the 11th Meeting of the International Association of Pancreatology (IAP) and the 35th Annual Meeting of the Japan Pancreas Society (JPS). Pancreatology. 2004;4(3-4):321-414. doi:10.1159/000079378

[2] Marchitti SA, Brocker C, Stagos D, et al. Aldehyde dehydrogenase 8A1: a novel retinaldehyde dehydrogenase that generates 9-cis-retinoic acid. J Biol Chem. 2008;283(49):33586-33595. doi:10.1074/jbc.M804210200

[3] Yin S, Bleul T, Zhu Y, et al. MiRNAs are unlikely to be involved in retinoid receptor gene regulation in pancreatic cancer cells. Cell Physiol Biochem. 2017;43(6):2449-2459. doi:10.1159/000485276

[4] Kaemmerer T, Stadler PC, Frommherz LH, et al. Alitretinoin in the treatment of cutaneous T-cell lymphoma. Cancer Med. 2021;10(20):7071-7078. doi:10.1002/cam4.4237

[5] Poizeau F, Balusson F, Jonville-Béra AP, et al. The cardiovascular safety of oral alitretinoin: a population-based cohort study involving 19 513 patients exposed to oral alitretinoin. Br J Dermatol. 2021;185(4):764-771. doi:10.1111/bjd.20069

[6] Del Aguila EM, Tang XH, Gudas LJ. Pancreatic ductal adenocarcinoma: new insights into the actions of vitamin A. Oncol Res Treat. 2022;45(5):291-298. doi:10.1159/000522425

[7] Yamakawa K, Koyanagi-Aoi M, Machinaga A, et al. Blockage of retinoic acid signaling via RARγ suppressed the proliferation of pancreatic cancer cells by arresting the cell cycle progression of the G1-S phase. Cancer Cell Int. 2023;23(1):94. doi:10.1186/s12935-023-02928-4

[8] Sun L, Zheng MF, Gao YH, Brigstock DR, Gao RP. Retinoic acid signalling pathway in pancreatic stellate cells: insight into the anti-fibrotic effect and mechanism. Eur J Pharmacol. 2024;979:176374. doi:10.1016/j.ejphar.2024.176374

[9] Del Aguila EM, Tang XH, Gudas LJ. Retinoic acid receptor-β deletion in a model of early pancreatic ductal adenocarcinoma (PDAC) tumorigenesis. Am J Cancer Res. 2025;15(1):127-140. doi:10.62347/xfot8509

[10] Gupta S, Rathore K, Tejavath KK. Understanding cytotoxicity induction by plumbagin in pancreatic ductal adenocarcinoma using network pharmacology, bioinformatic and in vitro study. Cytotechnology. 2026;78:46. doi:10.1007/s10616-026-00912-0

[11] Huang S, Gu D, Song D, et al. Integrating network pharmacology, molecular docking, and experimental validation to investigate the therapeutic effects and potential mechanisms of lycopene against pancreatic ductal adenocarcinoma. Front Nutr. 2026;13:1815515. doi:10.3389/fnut.2026.1815515

[12] Ma R, Xiao Y, Zhu W, et al. Single-cell and spatial transcriptomics uncover a THBS2* CAF-KRT17* malignant cell axis drives progression and immunotherapy resistance in pancreatic cancer. Transl Oncol. 2026;72(1):102939. doi:10.1016/j.tranon.2026.102939

[13] Parthiban R, Ekambaram B, Ravichandran V, et al. Integrative network analysis and molecular dynamics simulations identify silibinin as a putative modulator of EMT-ferroptosis crosstalk in pancreatic ductal adenocarcinoma. Cell Death. 2026;2(2):100010. doi:10.1016/j.celld.2026.100010

[14] Zhang Q, Cao Z, Yan S, et al. Spatial multi-omics defines cancer-associated fibroblasts subtype gradients driving metabolic support and immune remodeling in pancreatic ductal adenocarcinoma. Cancer Lett. 2026;653:218585. doi:10.1016/j.canlet.2026.218585